Int. J. Electrochem. Sci., 16 **(2021)** Article Number: 211251, doi: 10.20964/2021.12.21

International Journal of
ELECTROCHEMICAL
SCIENCE
www.electrochemsci.org

Evaluation and application of phytomass derived activated carbons as electrodes for coin cell supercapacitors

T. R. Banuprabha[1], A. Karthikeyani[2] and P. Kalyani[1,]*

[1] Department of Chemistry, DDE, Madurai Kamaraj University, Madurai, 625021, Tamil Nadu, India
[2] Department of Chemistry, Guru Nanak College, Chennai, 600042, Tamil Nadu, India
[*]E-mail: kalyani_1973@yahoo.com

Received: 24 July 2021 / *Accepted:* 23 September 2021 / *Published:* 10 November 2021

We report for the first time, a novel yet low-cost activated carbon (AC) derived from the leaves of Asian taro-AT and Indian shot-IS by conc. H_2SO_4 activation, followed by processing at 800^oC under N_2 flow for the possible application as electrodes in supercapacitors. Phase analysis, morphology, vibrational response and pore texture of the ACs were studied using standard techniques. Electrochemical features of ACs were evaluated by CV, GCD and EIS in 1M KOH. The calculated maximum capacitance tapped at the end of the 500th cycle was 348 F/g for ATAC and 259 F/g for ISAC at 10mA/g. Performance comparison includes the role of sulphur in ATAC recognizing mechanistic insights into material demands for supercapacitors. SC test coin cells were assembled to power LEDs to prove the utility of waste phytomass as electrodes in energy storage devices. The leaves have enormous prospects as supercapacitor electrode material supporting circular bioeconomy as well.

Keywords: Activated carbon, phytomass, pseudocapacitance, supercapacitor, circular bioeconomy, Asian taro, Indian shot

1. INTRODUCTION

The most important objective of today's sustainable development is to adapt to circular bioeconomy and to develop clean and reusable energy storage devices. The grave impacts of deprivation of fossils fuels, unattended pollution and the rapid growth of global economy have altogether resulted in the paradigm shift from linear economy to circular economy. Hence the advancement in electrochemical energy storage devices from natural and zero-cost materials with high electrochemical performance is the real challenge of the energy advocates. In support of these perspectives, carbon based materials such as activated carbons (ACs) [1], graphene [2], carbon nanospheres [3], metal oxides [4], conducting polymers [5] and polymer composites [6] have been proposed for energy storage devices such as supercapacitors (SCs), lithium-ion batteries (LIBs) etc.

SCs however are the inviting energy storage devices when compared to LIBs because of their distinguished properties like high gravimetric potentiality, perfect structural reliability, quick charge-discharge rates as well as long life-time [7].

SCs have an important role to play in various applications requiring power, such as hybrid electronic vehicles (HEVs), space ships, portable electronics, fast-acting short-term power backup for UPS, lasers and hand-held gadgets like digital cameras [8]. Categorization of SCs may be electrochemical double layer capacitors (EDLCs) and pseudocapacitors. In EDLCs the charges are stored through reversible ion adsorption at the electrode–electrolyte interface, while in the case of pseudocapacitors the charges are stored through redox reactions [9].

Among electrode materials presented above, carbonaceous materials possess significant properties including high electrochemical stability, adjustable porosity, large surface area, lightweight as well as cost effective and eco-friendly, the prerequisite features of an electrode material. Reasonable designs of electrode materials which include specific surface area, surface morphology and graphitization degree of the ACs are the significant factors to achieve excellent performance in terms of high specific capacitance, high charge/discharge rates and a long lifetime [7]. Considering these aspects, AC materials are the most demanding as electrodes in SCs.

It can be seen from the recent published literature that phytomass derived wastes are mainly utilized for synthesizing multifunctional ACs. Furthermore, phytomass are the origin of heteroatom dopants such as O, N, P and S representing the main sources for the performances of the ACs. The argument related with these wastes includes variations in quality along with accessibility, accumulation and transference from scattered areas [10]. In order to support sustainable technology, we have to decrease the consumption of natural resources or synthetic materials and search a origin of carbon involving wastes that is static in quality, produced in abundance and which can be easily assembled. In appreciation, the ACs produced from wastes could be aggressive or even perform finer than synthetically produced carbon materials.

It is well known that ACs is a form of carbon that has been refined to provide the possibility of large surface area, variable pore structure i.e. micro, meso and macro, high-degree of surface reactivity, conductivity, chemical inertness and physical stability. Because of these advantages, ACs have applications in different fields such as waste water treatment, pharmaceuticals, medicine, gold recovery, food industry, catalysis, gas separation, industrial purification etc [11]. Additionally, the large pore surface area and the cost-effective quality make them the largely favored functional material for the fabrication of electrodes and hence the potential of AC has been on the rise in energy storage sector [12] of late. Speaking of the sources of carbons, phytomass which are the carbon-rich organic sources are obviously the only popular natural precursor option for the production of high quality and better performing ACs at a reasonable cost. Thus utilization of waste phytomass has become one of the profound research avenues for carbon-based materials. To mention a few, researchers have utilized grape seeds [13] banana fiber [14], rice straw [15], garlic skin [16], waste tea [17], pineapple crown [18], eucalyptus bark [19], coffee grounds [20] for the synthesis of ACs for electrodes.

Despite innumerable investigation of phytomass to date, there are no optimization studies or direct theoretical data accessible to make or provide a rationale for choosing ACs with appropriate properties like structure, gravimetric or volumetric capacitance in connection with electrodes for SCs.

As a consequence, the exploration for carbon materials with enriched electrochemical nature is still being searched. It is evident that the aim of the present study is to explore novel and sustainable phytomass wastes viz., Asian taro-AT (*Alocasia odora*) and Indian shot-IS (*Canna indica*) which have no other value or advantage other than being planted for ornamental appeal have been utilized for deriving AC for SC electrodes and to appreciate the electrochemical behaviour in base (1M KOH) electrolyte. The suitability of these ACs is also demonstrated by fabricating test cells by lighting light-emitting diodes. Thus the work presented here not only supports circular bioeconomy by recycling wastes for value-added products but also expands the probability made available to us in the field of energy by our Nature for an important application.

2. MATERIALS AND METHODOLOGY

2.1. Materials

Alocasia odora (Asia Taro - AT) and *Canna indica* (Indian shot - IS) are the phytomass used as the precursors for the preparation of the AC powders. AT was collected near Vaigai dam, Tamilnadu, India and IS was collected at one of the author's home during autumn season. For the process, only leaves of the phytomass were used. Potassium hydroxide, Sulphuric acid-98% from Merck Ltd, carbon black, poly(vinylidene difluoride) (PVdF, MW = 450,000 g/mol), and N-methyl 2-pyrrolidone (NMP) were all purchased from Sigma-Aldrich, Stainless Steel-302 was used for fabricating electrodes on which coating of ATAC and ISAC slurry was done. The image of the two phytomass is given in fig.1.

Figure 1. Image of Asian taro - AT (*Alocasia odora)* (left) & Indian shot - IS (*Canna indica)* (right).

2.2. Synthesis of ACs (ATAC & ISAC)

In a typical procedure of synthesizing ATAC & ISAC, the leaves of the two phytomass were separated from the plants, washed with triple distilled water for several times and then dried under the sun for 3 days and powdered to 250 mesh. In a typical activation procedure, conc. H_2SO_4 was added to the samples for activation in the ratio of 1:1 (v/w) in a well cooled glass beaker and mixed well with a glass rod. Within a few minutes of adding the acid charring accompanied copious fumes. Oxygen deficient atmosphere was strictly maintained to avoid conversion of the precursors into CO_2. So after

cooling, the charred mass was carbonized at 800 ºC for 1 h at a ramp rate of 5 °C/min under flowing N_2 (flow rate: 5 mL/min) and this was done in an electric furnace with inner compartment made of quartz. At the same ramp rate, cooling was also done. To remove excess of activating agent and adsorbed matters, the resulting black lump was crushed to coarse powder and washed several times with triple distilled water. pH neutrality in the washings confirms the complete washing of the AC samples. Finally, an air oven was used to dry the black powder, then pulverized and was used for further characterization. The powders so obtained were named as Asian taro activated carbon and Indian shot activated carbon and designated respectively as ATAC & ISAC.

2.3. Activated carbon Yield and burn-off

The ratio of the mass of the AC (m_{ac}) to that of the dry and powdered biomass (m_d) results in % yield of the AC. % yield = (m_{ac}/m_d) × 100%, whereas the weight loss percentage due to the activation step gives burn-off. Burn-off = 100 - % yield.

2.4. Material characterization and EDLC testing

The surface morphology was investigated on S-3000H model microscope (SEM). The surface of the samples was degassed by running Ar gas as well as gold sputtering is done before scanning. X'Pert Pro X-ray diffractometer with CuKα (λ= 1.5406Å) radiation source was used to record X-ray diffraction patterns. X-ray intensity was measured in the range of $10^o<2\theta<80^o$ with a scan rate of 2^o/min. Surface functional groups of the ACs were determined employing FTIR spectrometer (Model # JASCO FTIR -5300) ranging from 4000 to 400 cm^{-1}. The pore framework of the ACs was identified by N_2 sorption at 77 K applying Micromeritics ASAP 2020 instrument (Micromeritics, USA). BET (Brunauer, Emmet and Teller) technique was followed to measure the surface area of the ACs. Vario ELIII CHNS/O Analyzer was used to carry out the elemental analysis of the ACs.

CH Instrument Model # CHI660a was used for electrochemical impedance spectroscopic (EIS), cyclic voltammetric (CV) as well as galvanostatic charge/discharge (GCD) studies. For the electrochemical studies (three electrode system), electrodes were furnished using SS rods with 8 cm length and circular ends of $1cm^2$ area. Electrode slurry was prepared by mixing the AC powders, commercial carbon powder and PVdF binder in the % weight ratio 88:10:2 with N-methyl 2 pyrrolidone as the solvent and was applied to the circular end of the SS rods. The electrodes were dried at 80°C for 1 h in vacuum oven. Heat shrinkable sleeve was used to mask rest of the electrode portion, leaving a small area at the top for establishing electrical connection with the electrochemical workstation. The working electrode is the SS rods coated with ATAC & ISAC, counter electrode is the platinum strip, and the reference electrode is Saturated Calomel Electrode. 25 ml of 1M KOH served as the electrolyte. Before measurements, the electrolyte was devolatilized with pure N_2 gas for nearly 10 min and during evaluation continuous out gassing occurred. The temperature of the solution was maintained at 28ºC by means of a water based thermostat.

2.5. Fabrication of coin cell prototype of supercapacitor

Symmetric supercapacitor test cells were fabricated in 2025 coin cell configuration using ATAC as a representative electrode material. Experimental slurry is resulted by mixing phytomass carbon with poly vinylidene fluoride binder and carbon black in the weight ratio 88:10:2 with N-methyl 2 pyrrolidone solvent. Aluminium foil of 20 μm thickness (also used as current collector) was taken and the slurry was coated uniformly on the foil with a brush. Then the foil was dried overnight under vacuum at 80^{o}C. In the next step, a pressure of 10 Kg/cm^{2} was applied using hydraulic press for complete adherence of the coated slurry on the top of the aluminum current collector. Following this, two discs of 1.6 cm diameter were punched out and weighed separately for finding the total mass of the materials on each current collector. Now the coated current collector is kept in vacuum oven at 80^{o}C continuously for 6 h and this step is done before fabricating SC coin cells. To eliminate air while fabrication, the cell fabrication was carried out in argon filled glove box. 2025 coin cell has two parts, the first one is "can" and the second one is "cap" both formed of SS. The two parts were dissociated by polypropylene "O" rings fixed to the cap. 20 mm in diameter is the cell dimension and 2.5mm is the thickness. Both identical weight electrodes were dissociated by polypropylene carbonate fabric separator. Now fixing this in the 2025-type coin cell, some drops of 1M KOH electrolyte were added. In order to remove the excess of air or oxygen, the cell was evacuated prior to electrolyte insertion and thus the wettability of the electrode surface is enhanced. Then to form supercapacitor coin cells the whole assembly was crimp sealed in a fly press. Before cell studies, the cells were ultimately kept aside without disturbance for 10 h to promote better soaking of the electrochemically active carbon sites in 1M KOH solution.

3. RESULTS AND DISCUSSION

3.1. Product yields and elemental analysis of activated carbons

The yield was calculated as 69% and burn-off as 31% for ATAC and 62% yield and burn-off 38% for ISAC. It can be stated that there will be decrease in % yield (AC) and raise in temperature would tend to raise the % burn-off. The % yield is quite significant such that the activation methodology adopted here is considered to be reliable and can be extended to any biomass or phytomass.

The nature, variety and % of the chemical ingredients are expected in determining the electrochemical variables and accordingly elemental analysis characterization technique was carried out. Results of the elemental analysis have been compared through fig. 2. ATAC has 3.374% N, 73.805% C, 1.018% H, 1.690% S and O+ash which was found out by difference as 20.113%, while ISAC was found to contain 2.356% N, 49.263% C, 2.426% H, 45.955% O + ash. It is well known that all these elements are coordinated in the form of many organic functional moieties, as will be discussed under FTIR results. % C in both the samples is not the same and % O is ~ 2 times more in ISAC. Interestingly, in ISAC no sulphur could be traced and hence the presence of sulphur in ATAC is considered to be significant in explaining any difference observed in the electrochemical performance

in the two ACs studied. For that reason, qualitative as well as quantitative studies on the hetero elements in ACs may prove an interesting and novel research topic in designing better performing AC.

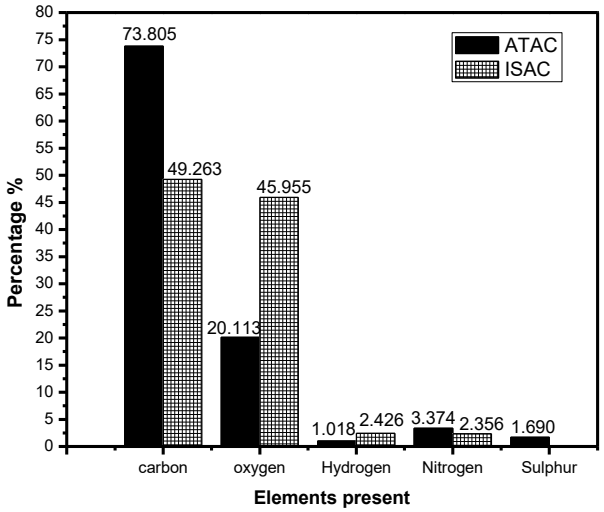

Figure 2. Elemental analysis of ATAC & ISAC.

The source of the hetero elements containing organic functional groups is obviously due to various active principles like triterpenoid glycoside, flavonoid C-glycosides, lignan glycosides, lignan and alkaloid are present in ATAC [21] and alkaloids, carbohydrates, proteins, flavonoids, terpenoids, cardiac glycosides, steroids, tannins, saponins, anthocyanin pigments, phlobatinins and many other chemical compounds are present in ISAC phytomass [22]. The presence of hetero elements improves the wettability and many other attributes of the carbon electrode, which in turn would be responsible for the overall electrochemical performance [23].

3.2. Characterization of phase and surface morphology

Phase analysis was executed through X-ray diffraction characterization technique. Both the samples present two broad diffraction peaks around 20~30° and 40~50°, characteristic of amorphous carbonaceous materials, which can respectively be ascribed to the (002) and (100) crystal plane diffractions. Figure 3(a) & (b) displays the XRD pattern of ATAC & ISAC. The broad peak at 25.4° in ATAC and peaks around 23.1° & 44.6º in ISAC exhibits the occurrence of honeycomb like framework established by sp^2 hybridized carbons [24] which also indicate that both the samples were formed by turbostratic carbon [25]. The peak positions were measured and 'd' spacing was calculated using Bragg's equation. The nature of the two peaks confirms the disordered nature and also the amorphous and graphitization features of both the samples. The graphitic structures may be due to the bond breaking of the organic components in the phytomass precursors. The interplanar space (d_{002}) computed for ATAC is 4.02Å and ISAC is 3.83Å, higher than graphite (3.354 Å) and this proves disorderliness or amorphousity [26] in both the samples selected for our study. The disordered

amorphous carbon shows diffuse scattering which reveals a large full width and half maximum (FWHM) which affirms the amorphous nature of ACs. [27]. Since the d_{002} value is higher for ATAC than ISAC, it is concluded that ATAC may be more amorphous than ISAC and that ATAC may exhibit better electrochemical performance than ISAC, a fact affirmed from the work of Kishore et al with coconut-kernel derived activated carbon [26].

In fig. 4(a) & (b), SEM images of ATAC & ISAC have been shown. As a result of activation of the phytomass, the micrographs show quite irregular cavities with heterogeneity on the external surfaces. The cavities are presumed to have resulted from the evaporation of H_2SO_4 during carbonization, leaving the spaces previously occupied by H_2SO_4 [28]. Ahmed et al [29] also have indicated that the heterogeneous structure might be probably due to the polymerization reaction (Scholl condensation reaction), occurring between aromatic hydrocarbons and tar-forming compounds in the structure of precursor during carbonization. Even though the cavities are heterogeneously distributed, this type of open structure can be effectively used for energy storage applications [29].

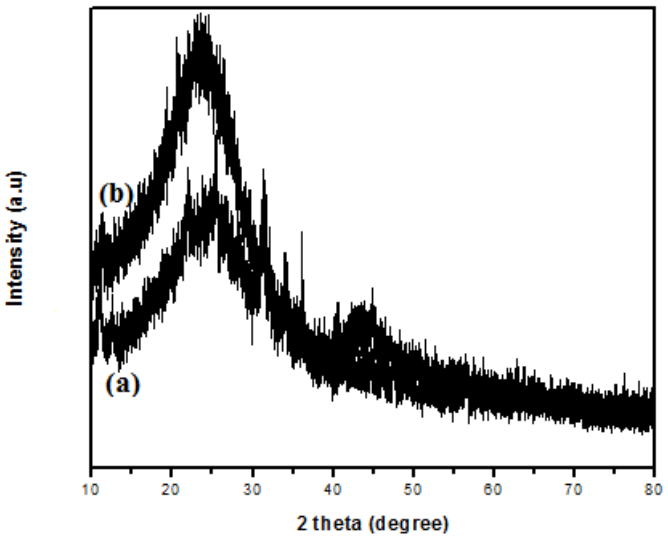

Figure 3. XRD of (a) ATAC & (b) ISAC.

SEM of ATAC vividly illustrate the pore-structure evolvement of the AC with numerous folds and depressions which explains the surface damage of AT. Further, the surface of ATAC shows a continuous network of pores and because of the presence of this continuous network of pores, an increase in the surface area, number of active sites and pore volume in AC is expected. The SEM of ISAC shows loose disjointed structures without any particular shape. It can be pointed out that H_2SO_4 activation enhances the deterioration of cellulose material and the aromatization of the carbon skeleton resulting in the creation of porous structures which is the platform for high electrochemical capacitance [30].

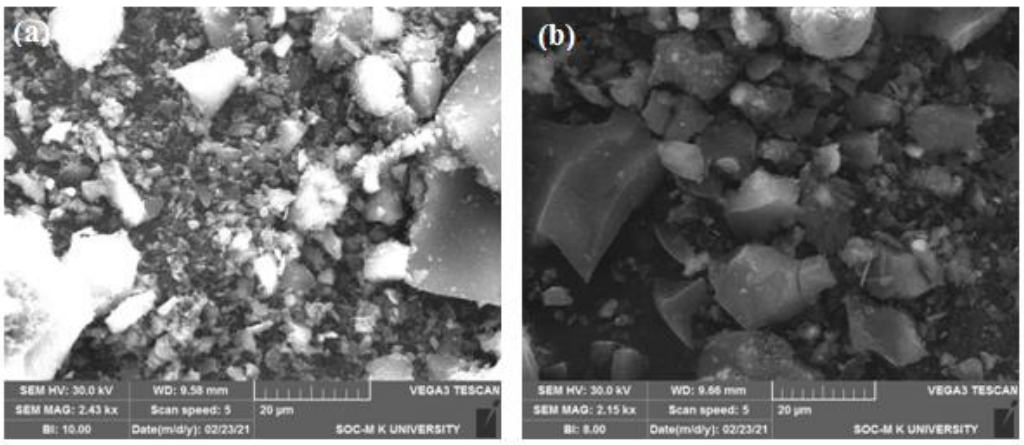

Figure 4. SEM of (a) ATAC & (b) ISAC at magnification 2K.

3.3. Functional group analysis by Infra red spectroscopy

FTIR vibrational studies are undertaken for the qualitative characterization of the various functional groups present on the ACs and are presented in fig. 5 (a) & (b). FTIR spectra shows the occurrence of alkyl groups, methyl groups, carbonyls, aldehydes, amides, amines, thiols and sulphide functional groups on the layers of the ACs and assignments of various FTIR signatures are listed out in Table 1.

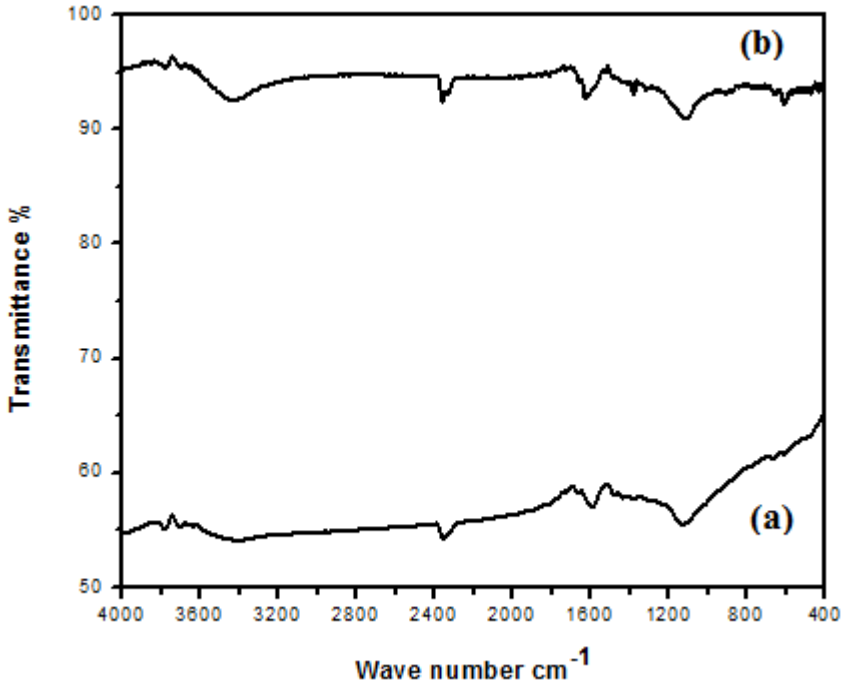

Figure 5. FTIR spectrum of (a) ATAC & (b) ISAC.

Table 1. FTIR peak analysis of ATAC & ISAC and their assignments.

ATAC		ISAC	
FTIR peaks (cm^{-1})	**Functional group/peak assignment**	**FTIR peaks (cm^{-1})**	**Functional group/peak assignment**
3780	Presence of OH group	3766	Presence of OH group
3410	-N-H vibration of amino group	3428	-N-H vibration of amino group
2910	-CH band of methylene group	2936	-CH band of methylene group
2515	-S-H stretching of thiols	2721	H-C=O stretching of aldehydes
2262	$-NH_2$ stretching of amides	2208	$-NH_2$ stretching of amides
1728	-C=O stretching of carboxylic acids	1717	-C=O stretching of carboxylicacids
1591	-NH vibration of amino group	1625	-NH vibration of amino group
1384	-S=O band of sulphoxides	1378	-CH band
1126	-C-O vibration of alcohol	1112	-C-O vibration of alcohol
611	-C-S band of sulphide	528	-C-H bending

The isolated –OH peak assignment is seen at 3780cm^{-1} for ATAC and 3766cm^{-1} for ISAC. The characteristic peak around 3410cm^{-1} for ATAC and 3428cm^{-1} for ISAC denotes the occurrence of -NH vibration of the amino group [31]. The assignment at 2910cm^{-1} for ATAC and 2936cm^{-1} for ISAC in the samples endorses the presence of aliphatic C–H bond corresponding to methylene group [32]. A band at 2515cm^{-1} for ATAC exhibits the existence of sulphur compounds [33] and a peak at 2721 cm^{-1} for ISAC assigns the occurrence of aldehydes stretching. The band at 2262cm^{-1} for ATAC and 2208cm^{-1} for ISAC shows the amide stretching. A peak around 1728cm^{-1} for ATAC and 1717cm^{-1} for ISAC shows the C=O stretches of carboxylic acids [15]. A characteristic peak observed at 1591cm^{-1} for ATAC and 1625 cm^{-1} for ISAC corresponds to N-H stretching vibration. A peak at 1384 cm^{-1} for ATAC shows the presence of sulphoxides [31] and 1378cm^{-1} shows C-H band [15] for ISAC. A peak at 1126cm^{-1} for ATAC and 1112 cm^{-1} for ISAC shows stretching of C-O group. A characteristic peak at 611cm^{-1} shows -C-S vibration in ATAC [17]. Thus FTIR spectroscopy clearly identifies a mixture of functionalities in both samples and as already mentioned, the additional sulphur containing groups in ATAC is likely to play an interesting and positive role towards determining/influencing the electrochemical behavior ultimately.

3.4. Textural properties and surface area analysis

The electrochemical performance of capacitors essentially depends on the surface properties and pore nature of the ACs. N_2 adsorption/desorption studies indicate the types of pores developed in ACs and the figs. 6 (a) & (b) is the N_2 isotherm of ATAC & ISAC respectively. According to IUPAC, there are six types of adsorption isotherms as type I to type VI classified based on the shapes of the isotherms obtained at different relative pressures (p/p_o). IUPAC also classifies the adsorbent pores into three groups viz, micropores (diameter < 2 nm), mesopores (2–50 nm) and macropores (>50 nm). The isotherm of ATAC has been identified to possess type IV characteristic where the isotherm shows a broad knee and hysteresis loop and also acquire type IV pore characteristics with micropores as well as

mesopores, according to the IUPAC classification. It is observed that the knee portion looks more rounded and displays hysteresis near $p/p_o = 0.7$. Hence for ATAC, type IV isotherm with hysteresis is reflected due to the presence of mesopores [34, 35]. For ISAC, the N_2 adsorption–desorption isotherm data show no hysteresis loop and belong to the type-I profile as classified by the International Union of Pure and Applied Chemistry (IUPAC), emulating huge microporosity [34, 36, 37]. This information concludes that chemical activation of phytomass sources is a successful method for preparing carbon powders with mesopores.

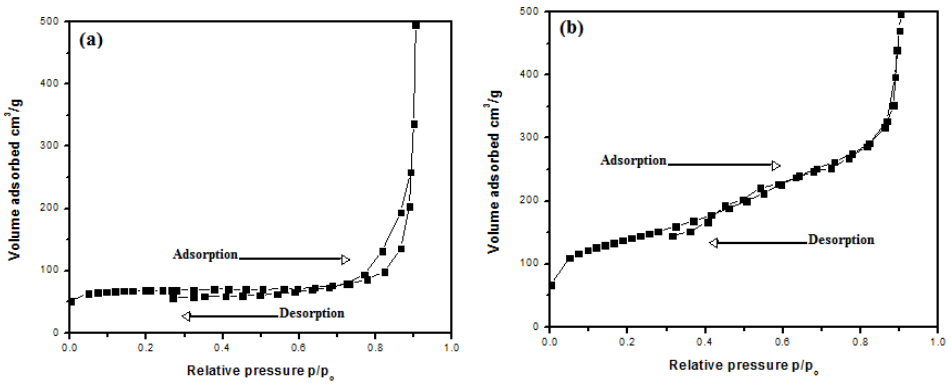

Figure 6. N_2 adsorption isotherms of (a) ATAC & (b) ISAC.

Table 2. Porous properties of ATAC & ISAC.

Sample designation	S_{BET} (m^2/g)	V_{total} (cm^3/g)	V_{meso} (cm^3/g)	V_{micro} (cm^3/g)	average pore width; 4V/A (nm)
ATAC	1215	1.36	0.85	0.51	4.5
ISAC	1103	1.06	0.61	0.45	3.8

Adsorption/desorption isotherms helps to calculate the Brunauer–Emmett–Teller (BET) surface area (S_{BET}) of ACs. Both total pore volume (V_{total}) and micropore volume (V_{micro}) were calculated by using t-plot method. By subtracting the V_{micro} from the V_{total} , we get mesopore volume (V_{meso}) [38]. These values along with the average pore width (4V/A) are compared in table 2. It is clear from table 2 that the pore structures formed in ACs is due to the combined effect of both meso and micropores. The mesopore volume accounts for 63% in ATAC & 58% in ISAC. This occurs due to the slow modification of micropores into mesopores during acid activation and amongst the two ACs examined, pore width of ATAC is found to be favorably larger than ISAC. These conclusions proves that ACs acquire large specific surface area and high mesoporosity with favorable pore width which might enhance the electrochemical behavior. As has been repeatedly mentioning that carbons produced from phytomass precursors possess high surface area, mesopore volume and are rich in heteroatoms, are helpful in creating enormous electrochemically accessible active sites, thereby conferring excellent electrochemical performance [39, 40]. Based on the above discussion, ATAC might be performing comparatively better than ISAC.

3.5. Electrochemical properties

3.5.1. Electrochemical impedance analysis

In electrochemical impedance spectroscopy EIS, Nyquist plots are the common representation of a. c. impedance. In general, the total impedance in the Nyquist plots may be sectioned into three regions according to a. c. frequency scanned (from milli to kilo Hertz) viz.,

(i) electrolyte solution resistance (R_s), which show up at high frequency region and depends upon the nature of the electrolyte used

(ii) interfacial charge transfer resistance (R_{ct}) between the electrode and the electrolyte, which can be identified by semicircle(s) at the middle frequency region and plays an important role in the electrochemistry of materials and

(iii) a straight line termed as the Warburg impedance (W) that occurs at low frequency region due to diffusion of ions into the intra-particle micropores of the electrode.

The existence of mesopores coupled with high electrical conductivity (low impedance), in addition to physical features is considered for developing electrode materials for energy devices.

Hence EIS study is conducted in 1M KOH electrolyte and is presented in fig. 7. It may be noted that for both the electrodes, a semicircle is observed. The semicircle is formed because of the porosity of the electrode and occurrence of resistance at the interface of electrode-electrolyte. A large semicircle indicates the resistance dominance at electrode-electrolyte interface, whereas the small semicircle shows the dominant capacitive nature [29]. Further for both the electrodes, in the intermediate frequency, a straight line segment is seen. A slope of approximately 45° in the intermediate frequency is also observed representing a union of resistive and capacitive behaviors due to the ions penetrating or diffusing into the pores of the electrodes. The degree of penetration of the ions in the electrolyte and the degree of accumulation of charges on the internal surface of the material electrodes depend on the pore nature of the AC, which in turn is known to be AC preparation procedure dependent processes.

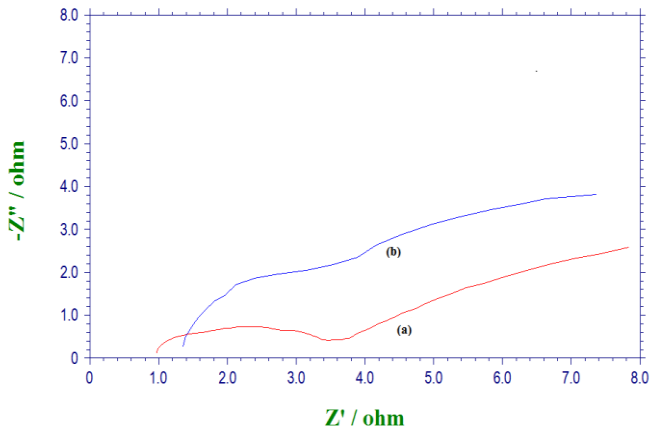

Figure 7. Nyquist plots of ATAC (a) & ISAC (b) electrodes.

From the Nyquist plot, the specific capacitance (C_{sp}) of the electrodes in base electrolyte was calculated using the formula $C_{sp} = 1/(2\pi fZ''m)$ and in this formula, f, Z'' and m denotes frequency (1mHz), imaginary impedance at f and mass of the carbon material respectively [41] and has been tabulated in table 3 along with R_s, R_{ct} and C_{sp} obtained in accordance with the Randles equivalent circuit. From the results of EIS studies, it can be inferred that resistance and diffusion barriers in the interior of the electrodes of ATAC is significant than ISAC and that in base electrolyte, C_{sp} is higher for ATAC than ISAC due to a low R_{ct}. Hence ATAC electrode materializes as a good capacitor electrode. The above conclusion for ATAC is also based on the facts that good ion transport, diffusion, conductive properties, presence of various heteroatoms and favorable electrode features such as enriched surface area and large mesopore volume, as examined in the preceding sections. Readers of this article may agree that the C_{sp} calculated from Nyquist plots are superior to the values obtained from many phytomass derived carbons reported [42].

Table 3. EIS data of ATAC & ISAC electrodes.

Sample designation	**R_s(Ω)**	**R_{ct}(Ω)**	**C_{sp} (F/g)**
ATAC	0.9	2.9	378
ISAC	1.3	3.1	306

So to conclude EIS studies, both the electrodes in 1M KOH exhibited the behavior of a capacitor with low internal resistance, thus indicating excellent electrolyte penetration/diffusion into the electrodes, augmented by mesopore development and higher surface area [43, 44].

3.5.2. Cyclic voltammetry

Electrochemical capacitance of ATAC & ISAC electrodes are investigated by CV studies in 1M KOH solution as electrolyte. KOH is most commonly used alkaline aqueous electrolyte because of its considerable conductivity of 540 mS/cm (H_2SO_4 & Na_2SO_4 has 750 & 91.1 mS/cm respectively) in the potential window 0-1V [45]. CV of the ATAC & ISAC electrodes scanned between 0 & 1V at various sweep rates from 10 to 50mV/s at the ending of the 5^{th} cycle is demonstrated in fig. 8 (a) & (b) respectively. In the base electrolyte, CVs show symmetric responses in both the scans without any redox peaks and the integrated stored charges in the positive scans will be furnished during the negative scans, thus proving better electrochemical nature of the two electrodes. It is also clear that when the scan is reversed, current rapidly reach plateau especially for ATAC. So this illustrates lower value of ESR (Equivalent series resistance) in the ATAC electrode in the base electrolyte chosen. It is well known that lower ESR is one of the prerequisites for higher capacitance retention at high currents and also the power capability of any electrochemical gadget [46].

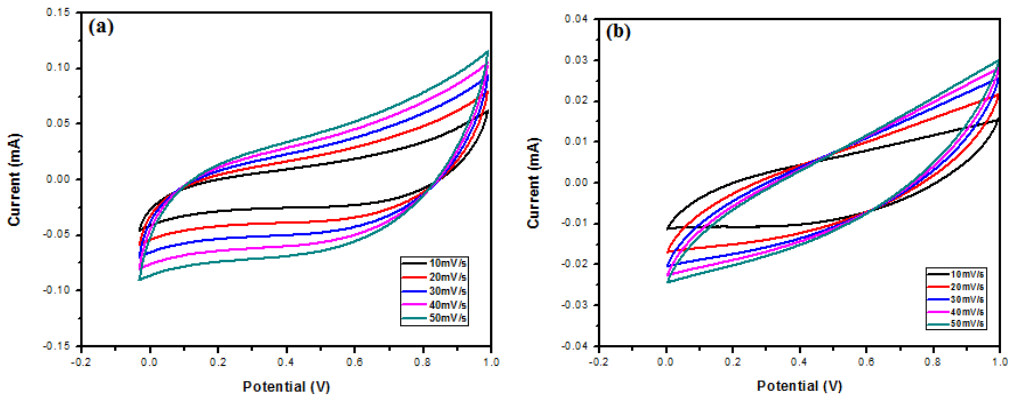

Figure 8. CV of (a) ATAC & (b) ISAC electrodes at different scan rates from 10 – 50 mV/s in 1M KOH.

It is also observed that in fig 8. that the capacitive currents of ATAC in 1M KOH is at least two times higher than that observed for ISAC. This may be explained by the fact that OH^- ions of the base electrolyte has electrochemically active and excellent mobility to approach the entire sample surface area of ATAC (because of high mesoporosity) over ISAC leading to quick charge distribution in ATAC. CV of ATAC & ISAC electrodes assume a distorted/quasi-rectangular shape unlike observed for an absolute EDLC, where perfect rectangular shape is seen.

It is interesting to find that in the basic medium, difference in electronegativity is due to the reaction of heteroatoms and carbon or hydrogen atoms present on the surfacial carbon [47]. KOH (the electrolyte used in the present investigation), is a highly polar compound, has a low affinity for carbon thus interacts strongly with heteroatom containing surface groups. Barzegar et al [48] have also reported that for AC electrode, KOH shows significantly good electrochemical behavior than neutral electrolytes like LiCl & Na_2SO_4. Furthermore, higher performance in KOH is due to its lower hydration radius (3.31 Å) and higher ionic conductivity (73 $cm^2/(\Omega .mol)$ in comparison to NaOH [49], where the Na^+ ion is with hydrated radius (3.58 Å) and conductivity 50 $cm^2/(\Omega .mol)$. The functional groups of carbon materials undergo Faradaic redox reactions and it has been affirmed in literature that the selected electrolyte is beneficial for the performance of self doped heteroelements and further enhance their pseudocapacitance [40]. So having these understanding as well, plausible interaction with various functional groups which are believed to occur is explained as follows, though the expected redox were not observed.

O-containing functional groups (e.g. C–OH, C=O & COOH) in AC enrich the pseudocapacitance contribution (in KOH electrolyte) thereby improving wettability and entire capacitance in supercapacitor electrodes [45]. The following are the plausible redox reactions in KOH electrolyte [45]:

$>C^*{-}OH + OH^- \leftrightarrow >C^*{=}O + H_2O + e^-$

$>C^*{=}O \leftrightarrow >C^*\text{-}O^- + e^-$

$>C^*OOH + OH^- \leftrightarrow >C^*OO + H_2O + e^-$

Redox mechanisms by which the N-containing functional groups can contribute towards pseudocapacitance in the phytomass derived ACs can be given as [50]

^^^C–NH_2 + $2OH^-$ ↔ ^^^C–NHOH + H_2O + $2e^-$

^^^CH–NH_2 + $2OH^-$ ↔ ^^^C=NH + $2H_2O$ + $2e^-$

where ^^^C stands for the carbon network of the ACs. Here N is believed to attract OH^- and improves the charge density of space charge layer [50].

Among the heteroelements, sulphur is the most active because of its lone pair and easily polarizable electrons and hence acts as a pseudocapacitance enhancer [17] in supercapacitors electrodes. The following two redox reactions are presumed to be responsible for pseudocapacitance [51]

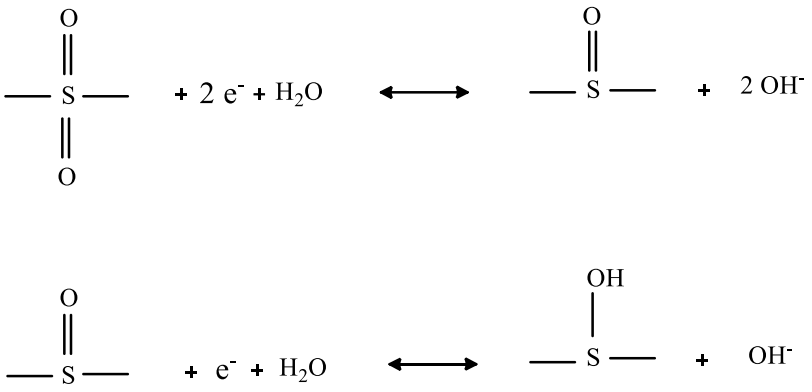

Despite the fact that, redox peaks were not observed in CV, it is believed that S-containing functional groups act as electron donors which is supposed to increase the conductivity [52] and provide adequate wettability to the electrode resulting in reduced diffusion resistance between the electrode and the electrolyte ions thus leading to fast ion transportation in to the pores of the electrodes [17]. Yet another reason attributed for pseudocapacitance is that the N-groups improve electrical conductivity and at the same time sulphur widens the interlayer spacing of the carbon structure to provide abundant electrochemical active sites [40]. This could be a reason why sulphur in ATAC (adds up with nitrogen) have a significant contribution towards electroactivity and hence pseudocapacitance eventually unlike ISAC where no sulphur could be traced. Thus, the overall capacitance is the synergy between sulphur and nitrogen, which again requires theoretical studies to confirm. It has been repeated in the literature that the electrochemical capacitance of the carbon materials used as electrodes is related to their pore type/size, electrolyte medium and also redox features due to the heteroatoms. As said above, the presence of various hetero atoms containing organic groups on the ACs particles surface explains the redox behavior of the ACs. Hence a clear prospect of the capacitor electrode with Faradaic character fabricated using ACs containing heteroatoms in base medium is demonstrated substantially by CV studies.

Table 4 gives the outcome of scan rates on the specific capacitance, C_{sp} of ACs estimated from the respective CVs at the end of the 5^{th} cycle applying the equation C_{sp} = I/S. In this equation 'I' denotes average current and 'S' denotes scan rate. The specific capacitance decreases with increasing scan rate as observed with many other AC electrodes. It can be contemplated that at high scan rates, the occurrence of EDL (electrochemical double layer) inside the pores of the carbon particles is slower and less complete in comparison to the lower scan rates [53]. Thus only at low scan rates the ions

transport/diffusion into the pores is facilitated to build up enormous charges and hence the capacitance. CV studies give that performance and the specific capacitance of ATAC in base electrolyte is higher than ISAC (but still in acceptable range), proving that ATAC could be optimized further for designing a prototype of a capacitor.

Table 4. Effect of scan rates Vs specific capacitance at 5^{th} cycle.

Scan rate (mV/s)	**Specific capacitance (F/g)**	
	ATAC	**ISAC**
10	380	310
20	369	298
30	355	277
40	338	262
50	321	239

Also, the authors of the present paper would like to list out a few reported work on various carbon samples. Misnon et al [47] have reported that oil palm kernel shell has delivered 210 F/g in 1M KOH at 0.5 A/g, Li et al [54] have reported that egg shell membrane exhibited 297 F/g in 1M KOH at 0.2 A/g. Peng et al [55] have tapped 245F/g in 2M KOH at 0.5 A/g from pomelo mesocarps. Thus the preliminary findings indicate that the performance of ATAC & ISAC is as good as the above. However, the enhanced capacitive behavior of ATAC over ISAC may be attributed, as described earlier, because of S-containing groups acting as a pseudocapacitance enhancer in addition to the improved physical features like surface area, mesopore volume, thus leading to a convincing increase in the overall capacitance value of ATAC.

To conclude CV studies, the scan rate as well as the nature of the carbon electrode materials influences the specific capacitance. The wettability, lipophilicity or hydrophilicity and electrical conductivity and electrolyte ion transport within the pores of the carbon materials is due to the surfacial functional moieties and this would be the ideal option for electrode materials in capacitors. As per the above discussion, it can be considered that ATAC as well as ISAC electrodes might be the ultimate choice as an electrode material in electrochemical capacitor devices.

3.5.3. Galvanostatic charge/discharge analysis

GCD technique is extremely useful for evaluating long term cycling stability of the electrodes at a particular current density. The electrochemical performance of ACs was explained by comparing their charge/discharge multi-cycling responses in the potential window of 0-1V at 10mA/g current density in 1M KOH as shown respectively in fig. 9 (a) & (b) where first 9 cycles is presented. The observed profile for both electrodes almost resembles to that of sawtooth shape, indicating their capacitive nature [29]. An isosceles trianglular shape was displayed in all charge–discharge curves which indicate high efficiency electrodes with low internal resistance and potential drop [56].

Generally for an ideal electrochemical capacitor, the expected curves for GCD are triangle in shape, with linear change in voltage/time, whereas in the case of pseudocapacitors, a non-ideal triangular shape is shown due to various redox reactions [57]. It is to be noted that the symmetry of the isosceles triangle is influenced by the difference in charge and discharge time. Thus the contribution of pseudocapacitance can be discovered with the linear and curved portion in the GCD curves demonstrating the combination of pseudocapacitance and EDLC.

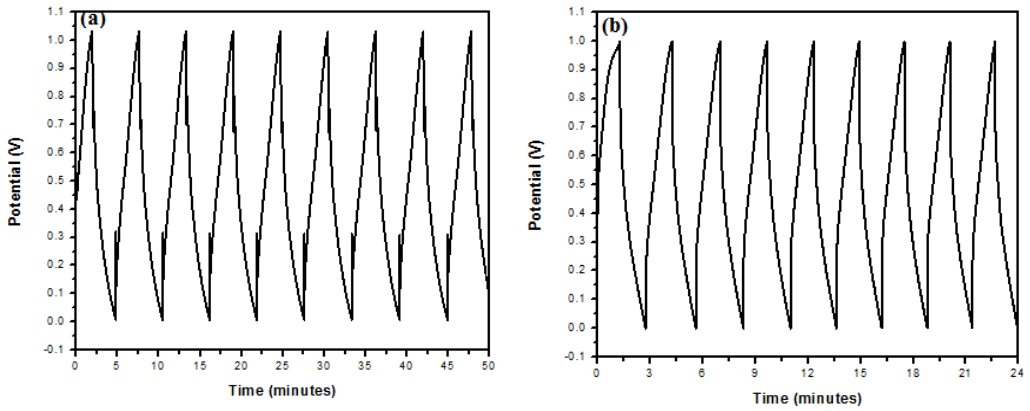

Figure 9. GCD profile of (a) ATAC & (b) ISAC recorded at 10mA/g in 1M KOH.

3.5.4. Cyclic stability

Cyclability of the two electrodes has been assessed up to 500 cycles and the specific capacitance Vs cycle number is listed in table 5. The charge-discharge curves gives the value of specific capacitance by employing the formula; $C = 2It/\Delta Vm$ (where C denotes single electrode specific capacitance of electrode material, t denotes the discharge time, I denotes discharge current, ΔV denotes voltage drop during discharge and m is the mass of electrode material in one electrode) [30]. The measured specific capacitance at the end of 500^{th} cycle is 348 F/g and 259 F/g for ATAC & ISAC. Also, the capacitance retention for ATAC & ISAC is 93 & 85% of the initial capacitance. From the readings below, it is deduced that ATAC electrode illustrated long-term cyclic stability with enhanced capacitance retention percentage.

Table 5. Specific capacitance Vs cycle number.

Cycle No.	Sample designation	
	ATAC	ISAC
1	375	305
50	372	301
100	369	297
150	366	295
200	363	289
250	360	285
300	357	279

350	355	275
400	351	269
450	349	266
500	348	259
% efficiency after 500 cycles	93.0	85.0

The polarity owing to the O-containing functional groups inhibits the ionic motion (electrolyte ions in meso/micropores) which may be really slow that the available micropores would not be employed for charge storage at high currents, in 10mA/g [58]. This leads to an important conclusion that the N- & S-containing groups have a major role in determining the overall capacitance of the electrodes. After scrutinizing the research reports present on phytomass derived activated carbon samples, it is noteworthy that leaves derived ACs gave a reasonably high and significant performance among many. Thus leaves derived ACs have successfully developed as an appropriate precursor for producing AC samples that too without any catalysts and templates, thus proving them as cost-effective capacitor electrode. Nevertheless, developing an efficient mesoporous carbon material electrode should include significant consideration on high rate charge-discharge capability [59] and mainly, quantification of the heteroatoms of the biomass derived carbons for a successful economically viable and green supercapacitor technology as our research should always be centered around circular bioeconomy and in that aspect, the authors of the present communication since quite recently has been focusing on the above concept for energy and few other applications.

3.5.5. Supercapacitor (SC) test cell studies

Studies have also been extended to confirm the potential of phytomass carbons by assembling symmetric SC 2025 coin type test cells using ATAC as the representative sample. To confirm the cycling stability, charge/discharge cycling studies were performed on the SC test cell. The capacitance value at the end of the first cycle was 370 F/g and the charge-discharge cycling was repeated for about 60 cycles and the values are plotted in fig.10. 95% of the initial capacitance was retained which infers that ATAC possess good electrochemical reproducibility and long-term cycle stability. Also for testing the feasibility in practical applications, the fabricated SC test cell was functioned to light three LEDs for 120 seconds unceasingly. The prototype cell with three LEDs is shown in inset of fig 10.

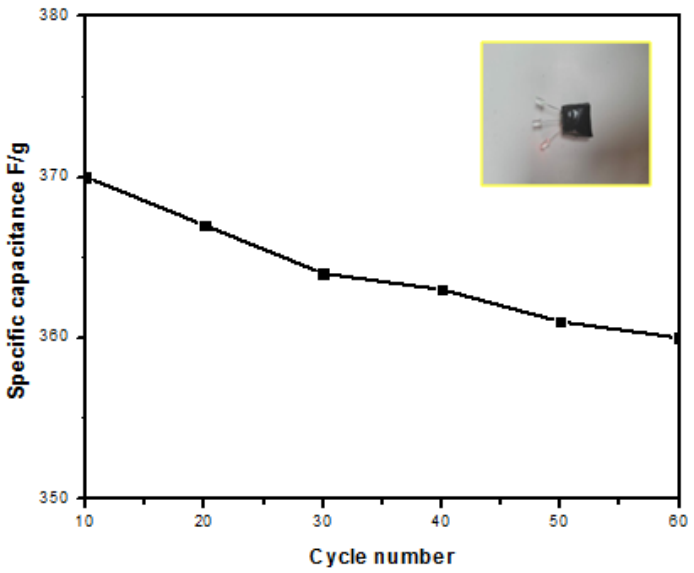

Figure 10. Cycle life data for ATAC. Inset: Three LEDs driven by fabricated SC test cell

4. CONCLUSION

The present study projected synthesizing a cost effective and eco-friendly AC from phytomass and assessed the suitability of the material as electrodes in supercapacitor. AC was derived from phytomass of Asian taro and Indian shot by employing chemical activation with conc. H_2SO_4 under N_2 flow. Phase analysis, surface morphology and vibrational response of the synthesized ACs were studied using standard techniques. Moreover, the capacitor performance of the two fabricated AC electrodes was compared in 1M KOH electrolyte. The highest specific capacitance value of 375 F/g at 10mA/g was obtained for ATAC electrode and further supercapacitor coin type test cell performance was also demonstrated with ATAC electrode by lighting LEDs. Among the various surfacial heteroelements present on the ACs, the presence of sulphur only in ATAC is believed to have a prime role in enhancing the capacitance via pseudocapacitance (ISAC has no sulphur). The authors of the present communication also presume that synergistic action of all the heteroatoms is expected to act nonetheless; a thorough qualitative and quantitative study should only decide the above argument, which by and large may assist identifying suitable AC. The synthesis reported herein also holds great potential for large-scale production of multifunctional carbon materials using various green and natural phytomass as starting materials thereby reinforcing circular bioeconomy. These advantages given here may also pave way to fabricate affordable AC-based materials for different advanced applications such as in photocatalysis, electrocatalysis, biosensors, microfluidic devices and hi-tech energy storage devices directing for future research.

ACKNOWLEDGEMENTS
The authors thank the management of Madurai Kamaraj University, Madurai for the encouragement to carry out this fundamental research at DDE. We express our gratitude to the experts at various Hi-end Institutes for characterizing the samples.

References

1. L. Hu, S. Liu, Y. Pan, L. Huang, Q. Cui, Y. Huang, J. Tang, W. Xu and J. Liu, *Int. J. Electrochem. Sci*., 16 (2021) 21065. https://doi.org/10.20964/2021.06.48
2. D. Ghosh and S.O. Kim, *Electron. Mater. Lett*., 11 (2015) 719. https://doi.org/10.1007/s13391-015-9999-1
3. GAM . Ali, S. Supriya , K.F. Chong, E.R. Shaaban, H. Algarni, T. Maiyalagan and G. Hegde, *Biomass Convers. Biorefinery*., 11 (2019) 1. https://doi.org/10.1007/s13399-019-00520-3
4. S.L. Kadam, S.M. Mane, P.M. Tirmali and S.B. Kulkarni, *Current Appl. Physics*., 18 (2018) 397. https://doi.org/10.1016/j.cap.2018.01.019
5. J. Wang, J. Wang, Z. Kong, Kuilin Lv, C. Teng and Y. Zhu, *Adv. Mater*., 1703044 (2017) 1. https://doi.org/10.1002/adma.201703044
6. B. Balli, A. Savk and F. Sen, *Woodhead Publishing Series in Composites Science and Engineering*., Chap 5 (2019) 123. https://doi.org/10.1016/B978-0-08-102509-3.00005-5
7. J. Wang, X. Zhang, Z. Li, Y. Ma and L. Ma, *J. Power Sources*., 451 (2020) 227794. https://doi.org/10.1016/j.jpowsour.2020.227794
8. S. Uppugalla and P. Srinivasan, *J. Solid State Electrochem*., 23 (2019) 295. https://doi.org/10.1007/s10008-018-4128-3
9. Z. Yu, L. Tetard, L. Zhai and J. Thomas, *Energy Environ. Sci*., 8(3) (2015) 702. https://doi.org/10.1039/C4EE03229B
10. Y. Boyjoo, Y. Cheng, H. Zhong, H. Tian, J. Pan, V.K. Pareek, S.P. Jiang, J.F. Lamonier, M. Jaroniec and J. Liu, *Carbon*., 116 (2017) 490. https://doi.org/10.1016/j.carbon.2017.02.030
11. S. Ahmed, M. Parvaz, R. Johari and M. Rafat, *Mater. Res. Express*., 5 (2018) 045601. https://doi.org/10.1088/2053-1591/aab924
12. R. Dubey and V. Guruviah, *Ionics*., 25 (2019) 1419. https://doi.org/10.1007/s11581-019-02874-0
13. I. Okmana, S. Karagöza, T. Tayb and M. Erdem, *Appl. Surf. sci*., 293 (2014) 138. https://doi.org/10.1016/j.apsusc.2013.12.117
14. V. Subramanian, C. Luo, A.M. Stephan, K.S. Nahm, S. Thomas and B.Q. Wei, *J. Phys Chem C*., 111 (2007) 7527. https://doi.org/10.1021/jp067009t
15. N. Sudhan, K. Subramani, M. Karnan, N. Ilayaraja and M. Sathish, *Energy & Fuels*., 31(1) (2016) 977. https://doi.org/10.1021/acs.energyfuels.6b01829
16. Q. Zhang, K. Han, S. Li, M. Li, J. Lia and K. Ren, *Nanoscale*., 10(5) (2017) 2427. https://doi.org/10.1039/C7NR07158B
17. S. Yaglikci, Y. Gokce, E. Yagmur and Z. Aktas, *Environ. Technol*., 41(1) (2020) 36. https://doi.org/10.1080/09593330.2019.1575480
18. E. Taer, A. Apriwandi, Y.S. Ningsih, R. Taslim and Agustino, *Int. J. Electrochem Sci*., 14 (2019) 2462. https://doi.org/10.20964/2019.03.17
19. N. Yadav, Ritu, Promila and S.A. Hashmi, *Sustain. Energy Fuels*., 4 (2020) 1. https://doi.org/10.1039/C9SE00812H
20. M. Biegun, A. Dymerska, X. Chen and E. Mijowska, *Materials*., 13 (2020) 3919. https://doi.org/10.3390/ma13183919
21. L.D. Viet, P.J. Houghton, B. Forbes, O. Corcoran and P.J. Hylands, *Planta Med*., 72 (2006). https://doi.org/10.1055/s-2006-949824
22. Ali Esmail Al-Snafi, *Int. J. Pharmacology & Toxicology*., 5(2) (2015) 71.
23. T.K. Enock, C.K. King'ondu, A. Pogrebnoi and Y.A.C. Jande, *Int. J. Electrochem*., 2017 (2017) 6453420. https://doi.org/10.1155/2017/6453420
24. M.R. Jisha , Y.J. Hwang, J.S. Shin, K.S. Nahmb, T. Prem Kumar, K. Karthikeyan, N. Dhanikaivelu, D. Kalpana, N.G. Renganathan and M. Stephan, *Mater. Chem. Phys*., 115 (2009) 33. https://doi.org/10.1016/j.matchemphys.2008.11.010

25. S.T. Senthilkumar, B. Senthilkumar, S. Balaji, C. Sanjeeviraja and R. Kalai Selvan, *Mater. Res. Bull*., 46 (2011) 413. https://doi.org/10.1016/j.materresbull.2010.12.002
26. B. Kishore, D. Shanmughasundaram, T.R. Penki and N. Munichandraiah, *J. Appl. Electrochem*., 44(8) (2014) 903. https://doi.org/10.1007/s10800-014-0708-9
27. A. Jain and S.K.Tripathi, *Ionics*., 23 (2014) 1391. https://doi.org/10.1007/s11581-014-1282-1
28. H. Demiral and I Demiral, *Surf. Interface. Anal*., 40 **(**2008) 612. https://doi.org/10.1002/sia.2716
29. S. Ahmed, A. Ahmed and M. Rafat, *J. Saudi. Chem. Soc*., 22 (2018) 993. https://doi.org/10.1016/j.jscs.2018.03.002
30. W.J. Si, X.Z. Wu, W. Xing, J. Zhou and S.P. Zhuo, *J. Inorg. Mater*., 26(1) (2011) 107. https://doi.org/10.3724/SP.J.1077.2010.10376
31. P. Kalyani, A. Anitha and A. Darchen, *Int. J. Eng. Sci. Res. Technol*., 4 (2015) 110.
32. M.S. Shamsuddin, N.R.N.Yusoff and M.A. Sulaiman, *Procedia Chem*., 19 (2016) 558. https://doi.org/10.1016/j.proche.2016.03.053
33. M. Danish, R. Hashim, M.N.M. Ibrahim, M. Rafatullah, T. Ahmad and O. Sulaim, *Bio Resour*., 6(3) (2011) 3019. Doi: 10.15376/biores.6.3.3019-3033
34. K.S.W. Sing, *Pure Appl. Chem*., 54(11) (1982) 2201. https://doi.org/10.1351/pac198254112201
35. T. Zhang, W.P. Walawender, L.T. Fan, M. Fan, D. Daugaard and R.C. Brown, *Chem. Eng. J*., 105 (2004) 53. https://doi.org/10.1016/j.cej.2004.06.011
36. S. Brunauer, P. Emmett and E. Teller, *J. Am. Chem. Soc*., 60 (1938) 309. https://doi.org/10.1021/ja01269a023
37. M.F.Y.M. Hanappi, M. Deraman, M. Suleman, N.S.M. Nor, N.E.S. Sazali, E. Hamdan, N.S.M. Tajuddin, N.H. Basri, M.R.M. Jasni and M.A.R. Othman, *Funct. Mater. Lett*., 10 (2017) 1750013. https://doi.org/10.1142/S1793604717500138
38. T.M. Chou and J.L. Hong, *Ionics*., 26 (2019) 1419. https://doi.org/10.1007/s11581-019-03261-5
39. G.Q. Zhang and S.T. Zhang, *J. Solid State Electrochem*., 13 (2009) 887. https://doi.org/10.1007/s10008-008-0623-2
40. A. Gopalakrishnan and S. Badhulika, *J. Power Sources*., 480 (2020) 1. https://doi.org/10.1016/j.jpowsour.2020.228830
41. D. Kalpana, S.H. Cho, S.B. Lee, Y.S. Lee, R. Misra and N.G. Renganathan , *J. Power Sources*., 190 (2009) 587. https://doi.org/10.1016/j.jpowsour.2009.01.058
42. L. Shi, L. Jin, Z. Meng, Y. Sun, C. Lib and Y. Shena, *RSC. Adv*., 8(70) (2018) 39937. https://doi.org/10.1039/C8RA08664H
43. L. Bonnefoi, P. Simon, J.F. Fauvarque, C. Sarrazin, J.F. Sarrau and A. Dugast, *J. Power Sources*., 80(1-2) (1999) 149. https://doi.org/10.1016/S0378-7753(99)00069-5
44. C.C. Ho, D.A. Steingart, J.W. Evan and P.K.Wright, *ECS. Trans*., 16 (2008) 35. https://doi.org/10.1149/1.2985625
45. R. Ramachandran and F. Wang, *Intechopen*., Chap 3 (2018) 51. https://doi.org/10.5772/intechopen.70694
46. B.E.Conway, *Kluwer Academic/Plenum Publishers*: (1999) New York, NY, USA
47. I.I. Misnon, N.M.K. Zain, R.A. Aziz, B. Vidyadharan and R. Jose, *Electrochim. Acta*., 174 (2015) 78. https://doi.org/10.1016/j.electacta.2015.05.163
48. F. Barzegar , D.Y. Momodu, O.O. Fashedemi, A. Bello, J.K. Dangbegnona and N. Manyala, *RSC. Adv*., 5 (2015) 107482. https://doi.org/10.1039/C5RA21962K
49. M.R.R. Abdul-aziz, A. Hassan, A.A.R. Abdel-aty, M.R. Saber, R. Ghannam, B. Anis, H. Heidari and A. S. G. Khalil, *IEEE Access*., 8 (2020) 200573. https://doi.org/10.1109/ACCESS.2020.3035828
50. S. He, H. Hou and W. Chen, *J. Power Sources*., 280 (2015) 678. https://doi.org/10.1016/j.jpowsour.2015.01.159
51. J. Huang, Zhang, H. Huang, Y. Liu, Q. Yang and L. Li, *ACS Sustainable Chem. Eng*., 7 (2019) 16710. https://doi.org/10.1021/acssuschemeng.9b04170

52. W. Kicinski, M. Szala and M. Bystrzejewski, *Carbon*., 68 (2014) 1. https://doi.org/10.1016/j.carbon.2013.11.004
53. A. Elmouwahidi, Z. Zapata-Benabithe, F. Carrasco-Mar´ın and C. Moreno-Castilla, *Bioresour. Technol*., 111 (2012) 185. https://doi.org/10.1016/j.biortech.2012.02.010
54. Z. Li, L. Zhang, B.S. Amirkhiz, X. Tan, Z. Xu, H. Wang, B.C. Olsen, C.M.B. Holt and D. Mitlin, *Adv. Energy Mater*., 2 (2012) 431. https://doi.org/10.1002/aenm.201100548
55. H. Peng, G. Ma, K. Sunb, Z. Zhang, Q. Yang and Z. Lei, *Electrochim. Acta*., 190 (2016) 862. https://doi.org/10.1016/j.electacta.2015.12.195
56. F.J. Liu, *J. Power Sources*., 182(1) (2008) 383. https://doi.org/10.1016/j.jpowsour.2008.04.008
57. K. Wang, H. Wu, Y. Meng, Y. Zhang and Z. Wei, *Energy Environ. Sci*., 5 (2012) 8384. https://doi.org/10.1039/c2ee21643d
58. E. Frackowiak and F. Beguin, *Carbon*., 39 (2001) 937. https://doi.org/10.1016/S0008-6223(00)00183-4
59. I. Yang, S.G. Kim, S.H. Kwon, M.S. Kim and J.C. Jung, *Electrochim. Acta*., 223 (2017) 21. https://doi.org/10.1016/j.electacta.2016.11.177